Comparison of optical vortex detection methods for use with a Shack-Hartmann wavefront sensor

Kevin Murphy[*] **and Chris Dainty**

Applied Optics Group, School of Physics, National University of Ireland, Galway
Galway, Ireland

[*]kevmurphy85@gmail.com

Abstract: In this paper we compare experimentally two methods of detecting optical vortices from Shack-Hartmann wavefront sensor (SHWFS) data, the vortex potential and the contour sum methods. The experimental setup uses a spatial light modulator (SLM) to generate turbulent fields with vortices. In the experiment, many fields are generated and detected by a SHWFS, and data is analysed by the two vortex detection methods. We conclude that the vortex potential method is more successful in locating vortices in these fields.

References and links

1. J. F. Nye and M. V. Berry, "Dislocations in wave trains," Proc. R. Soc. Lond. A **336**, 165–190 (1974).
2. J. F. Nye, *Natural Focusing and Fine Structures of Light* (Institute of Physics, London, 1999).
3. F. S. Roux, "Dynamical behavior of optical vortices," J. Opt. Soc. Am. B **12**, 1215–1221 (1995).
4. D. Rozas, C. T. Law, and G. A. Swartzlander Jr, "Propagation dynamics of optical vortices," J. Opt. Soc. Am. B **14**, 3054–3065 (1997).
5. V. V. Voitsekhovich, D. Kouznetsov, and D. K. Morozov, "Density of turbulence-induced phase dislocations," Appl. Opt. **37**, 4525–4535 (1998).
6. G. Gibson, J. Courtial, M. J. Padgett, M. Vasnetsov, V. Pasko, S. M. Barnett, and S. Franke-Arnold, "Free-space information transfer using light beams carrying orbital angular momentum," Opt. Express **12**, 5448–5456 (2004).
7. G. Gbur and R. K. Tyson, "Vortex beam propagation through atmospheric turbulence and topological charge conservation," J. Opt. Soc. Am. A **25**, 225–230 (2008).
8. B. J. Pors, C. H. Monken, E. R. Eliel, and J. P. Woerdman, "Transport of orbital-angular-momentum entanglement through a turbulent atmosphere," Opt. Express **19**, 6671–6683 (2011).
9. D. L. Fried and J. L. Vaughn, "Branch cuts in the phase function," Appl. Opt. **31**, 2865–2882 (1992).
10. H. Babcock, "The possibility of compensated astronomical seeing," Publ. Astron. Soc. Pac. **65**, 229 (1953).
11. R. K. Tyson, *Principles of Adaptive Optics*, 3rd ed, Optics and Optoelectronics (CRC Press, 2011).
12. B. C. Platt and R. Shack, "History and principles of Shack-Hartmann wavefront sensing," J. Refract. Surg. **17**, S573–S577 (2001).
13. J. Notaras and C. Paterson, "Point-diffraction interferometer for atmospheric adaptive optics in strong scintillation," Opt. Commun. **281**, 360–397 (2008).
14. E. O. Le Bigot and W. J. Wild, "Theory of branch-point detection and its implementation," J. Opt. Soc. Am. A **16**, 1724–1729 (1999).
15. W. J. Wild and E. O. Le Bigot, "Rapid and robust detection of branch points from wave-front gradients," Opt. Lett. **24**, 190–192 (1999).
16. K. Murphy, D. Burke, N. Devaney, and C. Dainty, "Experimental detection of optical vortices with a Shack-Hartmann wavefront sensor," Opt. Express **18**, 15448–15460 (2010).
17. G. A. Tyler, "Reconstruction and assessment of the least-squares and slope discrepancy components of the phase," J. Opt. Soc. Am. A **17**, 1828–1839 (2000).

18. D. L. Fried, "Branch point problem in adaptive optics," J. Opt. Soc. Am. A **15**, 2759–2768 (1998).
19. C. M. Harding, R. A. Johnston, and R. G. Lane, "Fast simulation of a Kolmogorov phase screen," Appl. Opt. **38**, 2161–2170 (1999).
20. R. A. Johnston and R. G. Lane, "Modeling scintillation from an aperiodic Kolmogorov phase screen," Appl. Opt. **39**, 4761–4769 (2000).
21. M. A. A. Neil, T. Wilson, and R. Juskaitis, "A wavefront generator for complex pupil function synthesis and point spread function engineering," J. Microsc. **197**, 219–223 (2000).

1. Introduction

Optical vortices (also called phase singularities, branch points or screw dislocations) are points on an optical wavefront where the phase is undefined and the intensity of the light drops to zero. Around these points the phase of the wavefront takes on all possible values from 0 to $\pm 2\,m\pi$ radians, where m is an integer corresponding to the charge of the vortex, leading to a spiral phase structure seen in Fig. 1. The sign of the vortex is defined by the direction of rotation of the phase around the singularity and is characterised as being either positive or negative. If the phase is defined over a range of 2π radians, as is commonly done in optics, then the phase of any wavefront with a vortex will be discontinuous. The phase of the wavefront will undergo a $\pm 2\,m\pi$ radian jump across the line of discontinuity, which will typically continue until it connects to another vortex of opposite sign. The basic properties of phase singularities in optics were observed by Nye and Berry in 1974 [1] and their structure in an optical field are systematically described in a later book by Nye [2].
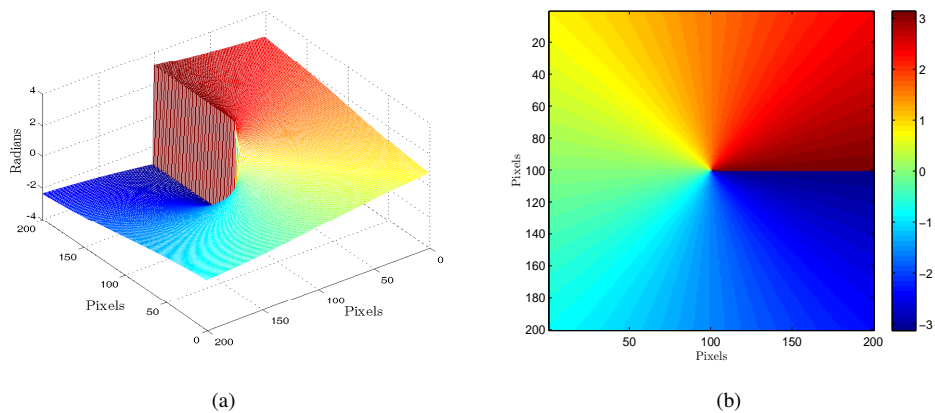

(a)	(b)

Fig. 1. Differing representations of a phase singularity, showing the spiral phase pattern, (a), and the line of phase discontinuity in an otherwise flat wavefront, (b), the colour bar is in radians.

Vortices occur naturally when the optical wavefront of a laser beam is heavily distorted, such as when the beam propagates through atmospheric turbulence, and can be seen in the plane of the receiver. Indeed vortices are so ubiquitous in nature that any speckle field will contain vortices where the intensity in the dark areas of speckle falls to zero. In such cases, vortices will be created in pairs of opposite sign (although one of the pair may be outside of the pupil and thus cannot be seen by the observer). The line of discontinuity which joins a pair of singularities is known as a wavefront dislocation (or branch cut). The propagation dynamics of vortices in a beam distorted by atmospheric turbulence have been studied by various authors [3,4] and it has been shown, through numerical simulations, that either increasing the propagation distance or increasing the strength of the turbulence leads to a larger number of vortices in the beam [5].

In some cases, for the purpose of optical communications systems, a beam may be deliberately seeded with one or more optical vortices [6]. For a single vortex this enables a three level system which could significantly reduce the bit error rate of the communications system as the vortex structure survives in the beam over long propagation distances [7]. Optical vortices are also being investigated for quantum communications systems for similar reasons [8].

Fried and Vaughan [9], focusing on the effects of distortion on an optical wavefront propagating through the atmosphere, showed that optical vortices and the associated wavefront dislocations are unavoidable in such conditions. They explained, and analytically quantified, the existence of these 2π dislocations in the phase function. This has implications for Adaptive Optics (AO) systems [10, 11], in reconstructing correctly the discontinuous wavefront and then implementing this discontinuous wavefront in hardware in the AO system.

A Shack-Hartmann wavefront sensor (SHWFS) is one of the most common and intuitive wavefront sensors used in AO systems [12] and is employed to obtain an estimate of the gradient of the distorted phasefront. This information can then be used to reconstruct the wavefront. The data can also be utilised to find the position and rotation of optical vortices in the field and two methods to do this will be outlined below. The SHWFS could also be applied to detect vortices in optical setups other than AO systems, for example in vortex communications systems. Other WFS can be used in atmospherically turbulent conditions, including the point diffraction interferometer which has been shown to produce promising results [13].

2. Detection methods theory

2.1. Vortex potential method

One method of detecting optical vortices in a field using a SHWFS is the vortex potential method which was first proposed by LeBigot and Wild in the late 90's [14, 15] (although the term branch point potential was used in their papers rather than vortex potential). This involves rotating all the phase gradient values calculated from the wavefront sensor by 90° and then form a potential plot of the resultant field, using a least squares reconstruction. The first step of this method is accomplished by performing a simple matrix multiplication to rotate the slopes,

$$R_{\pi/2}\,s = \begin{pmatrix} s_y \\ -s_x \end{pmatrix}, \tag{1}$$

where $R_{\pi/2}$ is a 90° rotation, s are the slope values measured by the wavefront sensor, with s_x and s_y the slopes x-values and y-values respectively.

The pseudo-inverse of the standard rectangular SHWFS geometry matrix is then calculated,

$$M' = (M^*M + m^2)^{-1}M^*, \tag{2}$$

where M^* is the adjoint of the geometry matrix and the m^2 value is inserted to prevent the matrix from becoming singular. It should be noted that this can be calculated in other ways including the singular value decomposition (SVD) method.

The potential function, V, is then calculated by multiplying the rotated slopes by the psuedo-inverse of the geometry matrix,

$$V = M'R_{\pi/2}\,s. \tag{3}$$

The potential function is reformed to match the shape of the lenslet array and can then be used to find the location of the optical vortices.

The positive vortices show up as peaks in the potential function and the negative vortices are seen as valleys in the potential function. In this method the peaks (and valleys) are identified by

being above (or below) a certain threshold value which is designed heuristically, although other methods could be used to define the peak (valley) position. The closer together vortex positions are in the field the more the peaks (valleys) shrink which can lead to masking of the vortices and more difficulty in detecting their positions.

LeBigot and Wild's work was done for numerically simulated data; we have previously shown that this method could be used on experimental data. Some early results for detection of vortices using the vortex potential method in the laboratory were presented [16].

2.2. Contour sum method

The most common method of detecting singularities in the phase function is the contour sum method, as recommended by Fried in 1992 [9], which is in essence a closed line integral over the gradient of the phase function,

$$\oint_C \nabla \phi \cdot \mathrm{d}l = \pm m 2\pi. \tag{4}$$

C denotes the closed integration contour, $\nabla \phi$ is the phase gradient and m represents the charge of the vortex enclosed. In practical terms a closed line integral is not convenient for the SHWFS as the contour sum involves the addition of measured phase gradients around in a closed loop. This summing of phase differences can be described mathematically as,

$$\sum(i,j) = s^x(i,j) + s^x(i,j+1) - s^x(i+1,j+1) - s^x(i+1,j)$$
$$- s^y(i,j) + s^y(i,j+1) + s^y(i+1,j+1) - s^y(i+1,j), \tag{5}$$

where $s^x()$ are the horizontal phase differences and $s^y()$ are the vertical phase differences.

If the phase is continuous i.e. no singularities present (or if there are two vortices of opposite sign enclosed by the loop of phase gradients canceling each other out) then this sum will be equal to zero (excluding noise). However if the sum around the loop is equal to, or a multiple of, $\pm 2\pi$ then there is a phase singularity enclosed in the loop. The sign of the $\pm 2\pi$ depends on the rotation of the screw type phase profile of the singularity. Traditionally the (i,j) th pixel is located at the top left of the four pixels.

The contour sum method has a number of assumptions which weaken its ability to detect vortices when used with a SHWFS setup. It assumes a closed circle of phase gradients around the addition loop; this is not the case with the SH slopes as they are formulated in the Fried geometry. It only uses four slope values to determine the presence of an optical vortex. These will be calculated, by definition, from the four closest SH spots to the position of the vortex making them more likely to have a low SNR, which leads to greater errors. Additionally, by convention, the vortex is placed at the (i, j) th aperture as a more exact position for the singularity is not established by this method. A more accurate vortex position could, presumably, be ascertained by using other techniques in combination with the standard contour sum method.

2.3. The slope discrepancy

The slope discrepancy technique is used to improve vortex detection by focusing on the curl of the vector potential. This approach is described by Tyler [17] and is defined mathematically as

$$\nabla \phi_{total} = \nabla \phi_{\mathrm{lmse}} + \nabla \phi_{\mathrm{sd}}, \tag{6}$$

where $\nabla \phi_{total}$ is the total measured gradient of the phase of the field, $\nabla \phi_{\mathrm{lmse}}$ is the gradient of the least-squares phase and $\nabla \phi_{\mathrm{sd}}$ is the gradient of the slope discrepancy part of the phase.

It is obvious that Eq. (6) is closely related to the hidden phase introduced by Fried [18] and, in fact, only differs as measurement noise and fitting errors are included in the slope discrepancy along with the phase associated with phase singularities. This provides a powerful technique to aid in the detection of vortices, as using this approach along with either vortex detection method should improve the chances of detection. A published paper shows this to be the case for the vortex potential method [16] and all results presented here make use of the slope discrepancy.

3. Experimental work

3.1. Optical setup

The experimental method and the optical setup used for these experiments is the same as in [16] and therefore shall only be dealt with briefly here. A schematic of the optical system used to conduct the experiments is displayed below, Fig. 2.

Fig. 2. Schematic of the complete optical setup built and used experimentally in the laboratory, with the various beams shown.

A HeNe laser is collimated using L1 and propagated into the system before being split by a 50:50 beamsplitter with one beam continuing straight (reference beam) and the other entering the SLM arm. The reference beam goes through the beamsplitters BS3 and BS4 and into the optical trombone which is used to change the conjugate of the SLM image plane along the beam path.

The SLM beam is directed onto a ferro-electric SLM which is used to create phase singularities and mimic the effects of atmospheric distortion in the beam with phase screens generated using numerical methods [16, 19, 20]. The SLM works on the principle of binary phase modulation, with the values of 0 and π radians used here [21]. The SLM utilised in the setup is from Boulder Nonlinear Systems, has a refresh rate of up to 1015 Hz and a pixel size of 15 μm, with

512×512 pixels in total.

The SLM reflects the beam which then travels through L4 and L5 and an iris, which is used to pick off the $+1$ diffraction order of the SLM image in the Fourier plane. It exits the arm through BS4 then travels through the optical trombone and joins the reference beam. After the beams combine interferometry can be accomplished if a flip mirror, FM1, is in a certain position.

When interferometric images are needed the flip mirror is flipped up into the path of the beam and it redirects the beam into lenses L8 and L9 which demagnify the image onto the interferometry CCD camera. When measurements involving the Shack-Hartmann sensor are needed then FM1 is flipped down out of the beam path and the reference beam is blocked off somewhere along the its path, while the SLM beam continues into the wavefront sensing arm.

The wavefront sensing arm is primarily used to measure the beam coming from the SLM arm. The Shack-Hartmann wavefront sensor itself comprises of the lenslet array, the relay lenses L12 and L13 and a CCD camera, CCD2. The lenslet array is a refractive microlens array, with 50×50 lenslets, pitch of 100 μm and a focal length of 2.7 mm. This short focal length necessitates some relay optics between the array and the detector, a QImaging Retiga EXi CCD camera with 1392×1040 pixels of pitch 6.45 μm $\times$ 6.45 μm and a digital output of 12 bits.

4. Results for detection of optical vortices

4.1. *Experimental measurements*

The measurements taken involved using simulated atmospheric turbulence wavefronts of various strengths, ranging from r_0 sizes of ≈ 80 cm to ≈ 4.7 cm and from σ_I^2 values of ≈ 0.04 to ≈ 1.904, where the normalised intensity scintillation is, $\sigma_I^2 = \frac{\langle I^2 \rangle - \langle I \rangle^2}{\langle I \rangle^2}$. The relationship between these sets of values are shown in Fig. 3 and in Table 1 below. Experimental measurements are acquired for phase distortions only and for phase and intensity distortions combined for each of these turbulence levels. A series of four different Shack-Hartmann spatial samplings were used to examine how this effects optical vortex detection for the SHWFS. These extend from 1.655 cm/lenslet to 0.2758 cm/lenslet and are detailed in Table 1. The difference in sampling is achieved by changing the number of discrete points of the phase and intensity wavefronts applied to the SLM while keeping the area utilised on the SLM constant.

Table 1. The relationship between the range of values used for the coherence length, r_0, and the intensity scintillation, σ_I^2, in the experiments. The four separate SH lenslet samplings used are given.

Parameter	Range of Values Used						
Coherence Length, r_0 (cm)	80	32	21	11	8	5.7	4.7
Scintillation, σ_I^2	0.04	0.18	0.56	1.03	1.45	1.75	1.90

Parameter	Range of Values Used			
SH Sampling (cm/lenslet)	1.68	0.83	0.55	0.28

4.2. *Effect of atmospheric phase distortions and intensity scintillation on vortex detection*

This section deals with the effect of the phase aberrations and intensity scintillations of the atmospherically distorted wavefronts produced by the SLM have on optical vortex detection. The vortex detection ability of the vortex potential method is compared to that of the standard contour sum method. The vortices which are examined here are either the only optical vortex in the field or are spatially well separated from other vortices present in the field. This is to
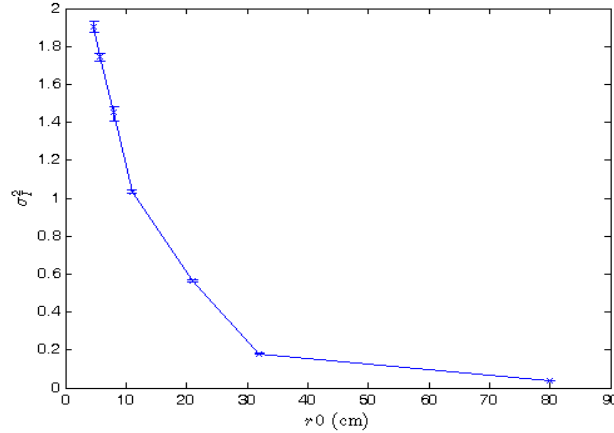
Fig. 3. The normalised intensity scintillation, σ_I^2, plotted against the approximate coherence length, r_0, for the wavefronts used in the experiments. The error bars on the σ_I^2 values correspond to the maximum and minimum intensity scintillation for the various degrees of Shack-Hartmann sampling.

differentiate the problem of basic vortex detection from that of the ability to resolve vortices which are close spatially, such as vortex pairs, which is dealt with later in Sec. 4.3.

Below the correct detection of these vortices is plotted against the coherence length, r_0, and the normalised intensity scintillation, σ_I^2, values of the different wavefronts for varying degrees of sampling. A correct detection of a vortex is defined as one which finds accurately the sign and position of the vortex in the field while giving no false positive detections. The two data sets shown in the following graphs correspond to all of the correct detections given by the vortex potential method (blue line) and to all of these correct detections which given by the contour sum method (red line). This is done for both the full optical field case and the phase aberration only case, which has the same phase aberrations but uniform intensity across the field.

Figure 4 illustrates the percentage of correct vortex detections against the coherence length, r_0, for the phase only case. This is done for the four different sampling levels outlined in Table 1, with sampling increasing from Fig. 4(a) through to Fig. 4(d). This figure compares the vortex detection rate for the vortex potential method and the contour sum method. The blue line is the vortex potential detection rate and the red line is the contour sum vortex detection rate.

When the detection rate drops to zero in Fig. 4 it is due to the high degree of phase aberration which causes the SH spot to blur and enlarge and spot motion becomes substantial. These effects combine to overcome the dynamic range of the SHWFS for that particular SH lenslet sampling level. What should be noted from Fig. 4 is that the contour sum method does not perform as well as the vortex potential method for any degree of phase abberation or sampling level. The data presented in Fig. 4 is reproduced in Table 2.

Figure 5 shows the percentage of correct detections against the Shack-Hartmann sampling level for six coherence lengths. This is done for the vortex potential method (blue) and the contour sum method (red). It is performed for the case of phase aberrations only. The six coherence length values, r_0, used are 80 cm, 32 cm, 21 cm, 11 cm, 8 cm and 4.8 cm which correspond to Figs. 5(a), 5(b), 5(c), 5(d), 5(e) and 5(f) respectively. The general trend for the vortex potential method show that the finer the sampling level the greater the amount of correct detections, especially at higher turbulence levels. This trend is not as evident for the case of the contour sum method. This may be explained by the threshold level for vortex detection using the contour

Table 2. The data used in Fig. 4 comparing how the contour sum method performs for the case of phase aberrations only over the four SH sampling levels shown against the vortex potential method. The data highlighted in grey is that for the vortex potential method, with the data in white is the detection rate for the contour sum method.

Fried's Parameter, r_0 (cm)	80	32	21	11	8	5.7	4.7
% Correct Detections	100	40	-	-	-	-	-
Sampling 1.68 cm/lenslet	65	0	-	-	-	-	-
% Correct Detections	97	73	36	24	-	-	-
Sampling 0.83 cm/lenslet	27	40	16	2	-	-	-
% Correct Detections	100	93	93	67	20	-	-
Sampling 0.55 cm/lenslet	54	44	38	11	0	-	-
% Correct Detections	100	100	100	93	87	93	73
Sampling 0.28 cm/lenslet	9	26	20	36	27	27	7

sum method needing to be re-optimised for each individual SH sampling level.

In Fig. 6 the percentage of correct vortex detections is plotted against both the coherence length, r_0, and the normalised intensity scintillation, σ_I^2, for the full optical field case. This is done for the four different sampling levels in the same way as in Fig. 4, with the sampling increasing from Fig. 6(a) through to Fig. 6(d). Here the vortex potential method detection rate (blue) and the contour sum method detection rate (red) are shown. Again when the detection rate drops to zero it is due to the strength of the phase aberrations and intensity scintillation overcoming the dynamic range of the SHWFS for that particular Shack-Hartmann sampling level.

While Fig. 6 appears to be similar to Fig. 4, there are differences when looking at the full optical field case as opposed to the phase only case. The key differences from Fig. 6 are that while weak intensity scintillation appears to have little effect on vortex detection, moderate to strong intensity scintillation does decrease the vortex detection rate, even for the vortex potential method. It is shown again that the contour sum method performs considerably worse than the vortex potential method for all cases, following the pattern identified in Fig. 4. The data corresponding to Fig. 6 is presented in Table 3.

The percentage of correct detections against the Shack-Hartmann sampling level for six coherence lengths, and their associated intensity scintillations, σ_I^2, are given by Fig. 7. This is again done for both the vortex potential method detection rate (blue) and the contour sum detection rate (red). The six coherence length, r_0, values used are 80 cm, 32 cm, 21 cm, 11 cm, 8 cm and 4.8 cm for Figs. 7(a), 7(b), 7(c), 7(d), 7(e) and 7(f) respectively. The intensity scintillation, σ_I^2, values used are 0.04, 0.18, 0.56, 1.03, 1.45, 1.75 and 1.9 for Figs. 7(a), 7(b), 7(c), 7(d), 7(e) and 7(f) respectively. The same general trend, as seen in Fig. 5, emerges for the vortex potential method with the finer the sampling level the greater the amount of correct detections. Similarly, for the contour sum method, the finer SH sampling does not necessarily mean better vortex detection, which again could be explained by the possibility that the threshold of detection for contour sum method may need to be re-optimised for each individual Shack-Hartmann sampling level.

As an aside it should be noted that it was attempted to improve the effectiveness of the vortex potential method by also taking into account the intensity pattern of the Shack-Hartmann spots. At the location of a vortex the Shack-Hartmann spot will take on the characteristic annular shape of an optical vortex, by creating an annular template and using a matched filter technique, the
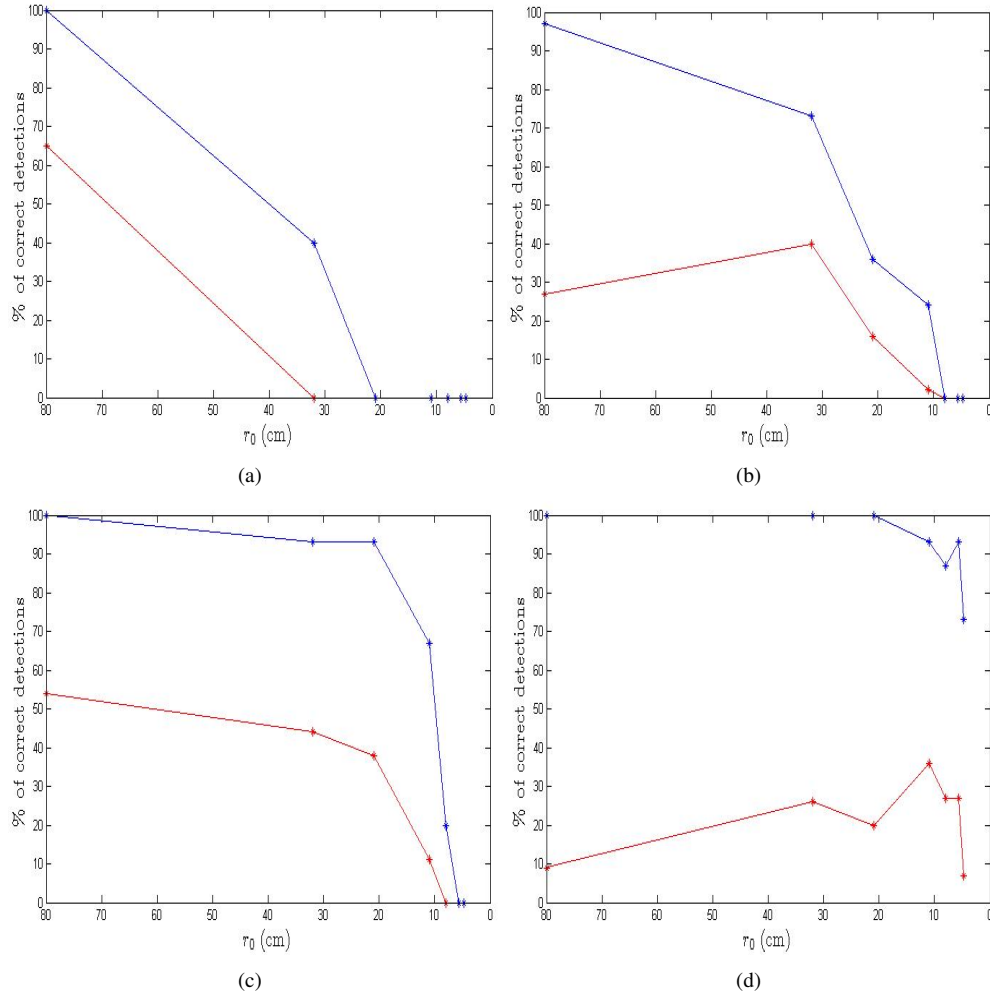
Fig. 4. Graphs of the percentage of correct detection of vortices against the coherence length, r_0, for the vortex potential (the blue line) and the contour sum (the red line), for the case of phase aberrations with uniform intensity. The SH sampling level is 1.68 cm/lenslet for (a), 0.83 cm/lenslet for (b), 0.55 cm/lenslet for (c) and 0.28 cm/lenslet for (d).

detections made by the vortex potential could be confirmed. This was done by checking spots in the immediate vicinity of the detection and seeing if they conform to the annular shape. This, however, did not have a large impact on the vortex detection rate but did lessen the amount of false positives recorded. The technique encountered difficulties when the spatial sampling was increased and the annular pattern was spread over a larger number of lenslets; this also made the technique more susceptible to intensity scintillation effects. There does remain a capacity for using the intensity information (or lack thereof) of Shack-Hartmann spots in aiding the detection of optical vortices in such a system.

4.3. Lenslet separation needed for vortex detection

This section presents the Shack-Hartmann spatial lenslet separation needed to resolve a pair of oppositely signed vortices for the contour sum method compared to the vortex potential
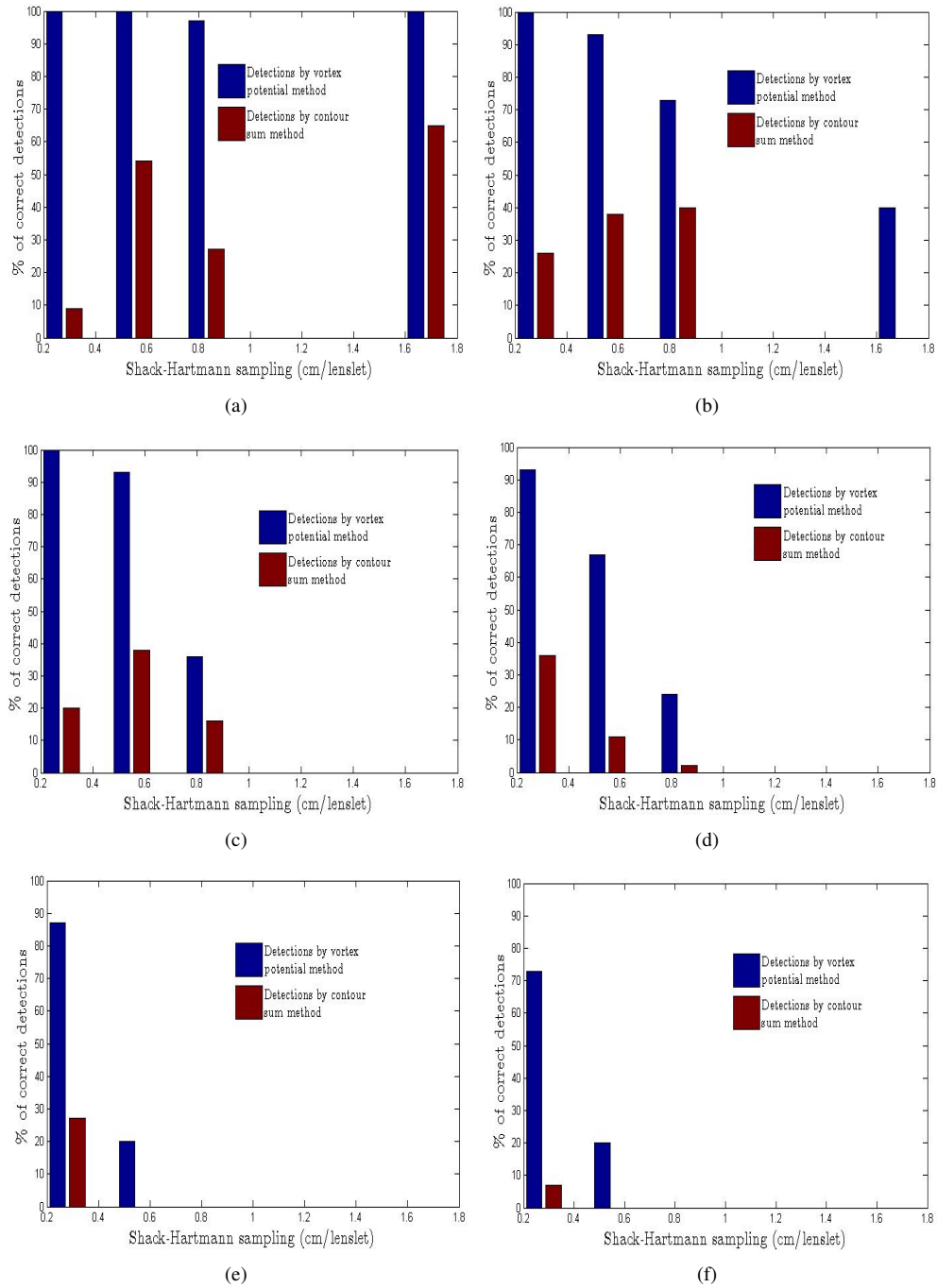
Fig. 5. Percentage of correct detections against SH sampling levels for the contour sum method for six different r_0 levels; 80, 32, 21, 11, 8 and 4.8 cms for (a) through to (f) respectively.
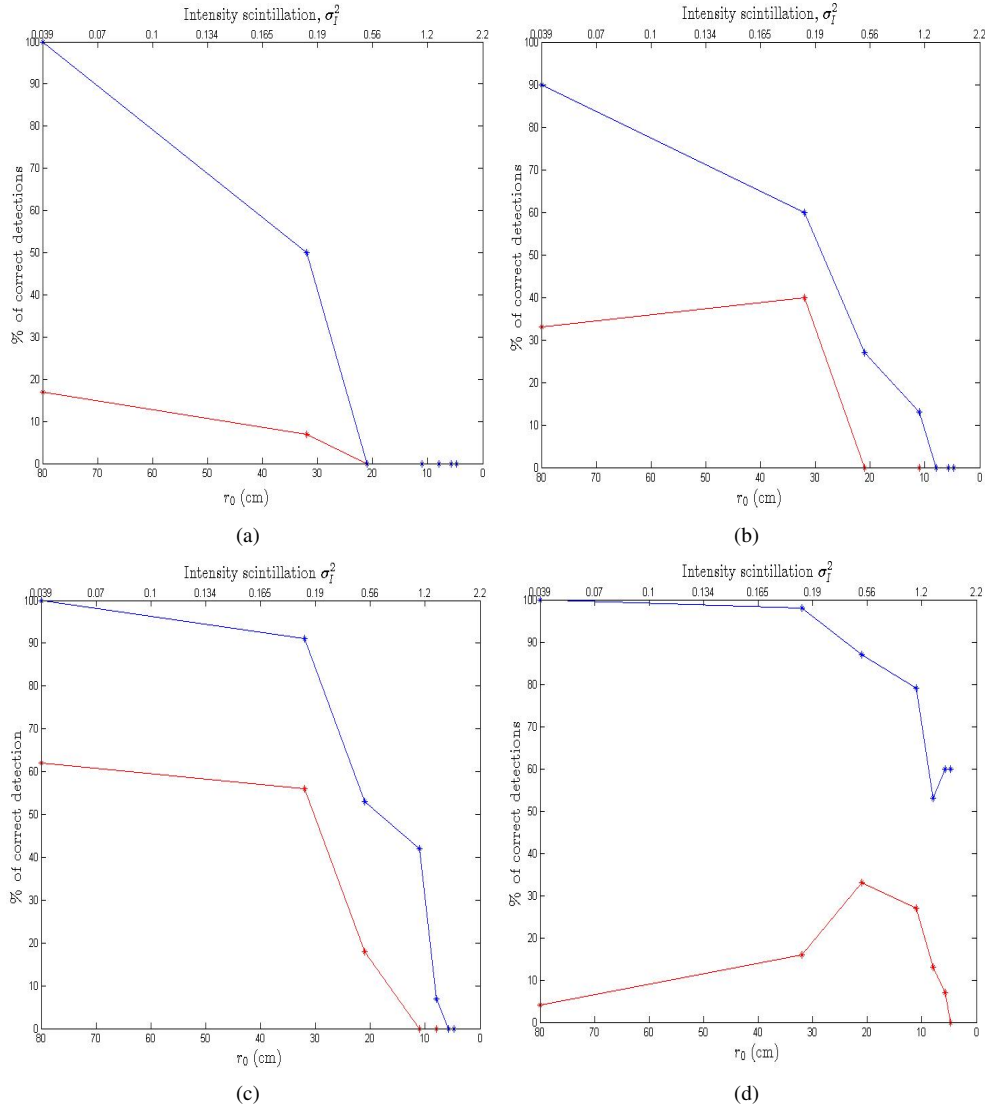
Fig. 6. The percentage of correct detection of optical vortices against the coherence length, r_0, and the intensity scintillation, σ_I^2, for the vortex potential method (blue line) and the contour sum method (red line), for the case of the full optical field. The Shack-Hartmann sampling level for each of these graphs is; 1.68 cm/lenslet for (a), 0.83 cm/lenslet for (b), 0.55 cm/lenslet for (c) and 0.28 cm/lenslet for (d).

method. The spatial separation of the pair is given in terms of Shack-Hartmann lenslets. In the case presented here the minimum lenslet separation needed is found for a $r_0 = 80$ cm and, when the full field is used, a $\sigma_I^2 = 0.04$. In Fig. 8 the vortex potential data for vortex separation is in blue and the data for the contour sum method data is in red. Table 4 displays the data used in Fig. 8(a) and Table 5 the data used in Fig. 8(b).

The results illustrated in Fig. 8 and the associated Tables show the contour sum method does not detect vortex pairs as well as the vortex potential method; this is to be expected going on earlier results. Closer inspection, especially of Fig. 8(b), reveals a dip in the vortex potential
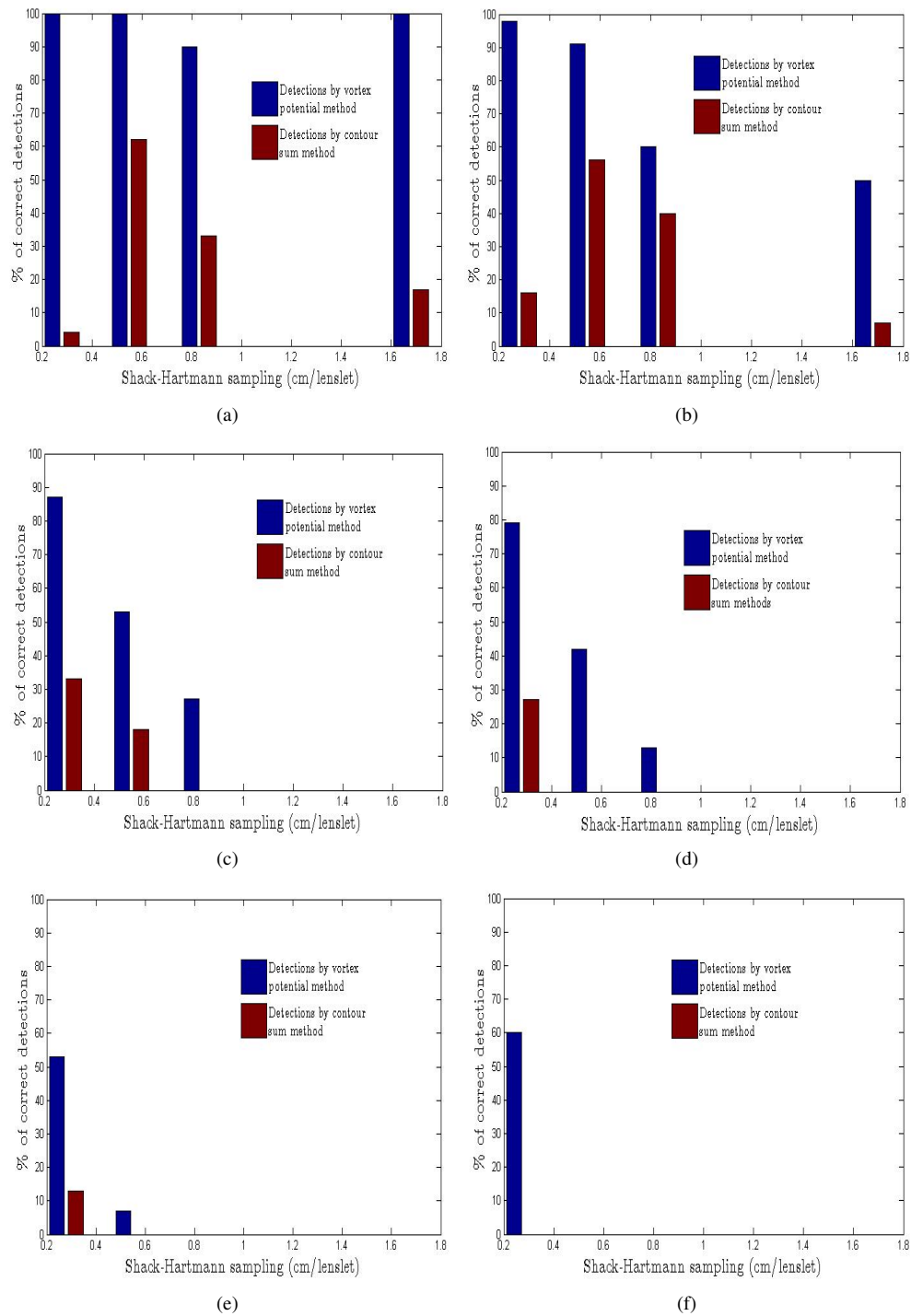
Fig. 7. Percentage of correct detections against SH sampling levels for the contour sum method for six different coherence lengths, r_0; 80 cm, 32 cm, 21 cm, 11 cm, 8 cm and 4.8 cm, and their associated intensity scintillations, σ_I^2; for (a) through to (f) respectively.

Table 3. The data used in Fig. 4 comparing how the contour sum method performs for the full optical field case over four SH sampling levels to the vortex potential method. The data in grey is that for the vortex potential method, with the data in white is the detection rate for the contour sum method.

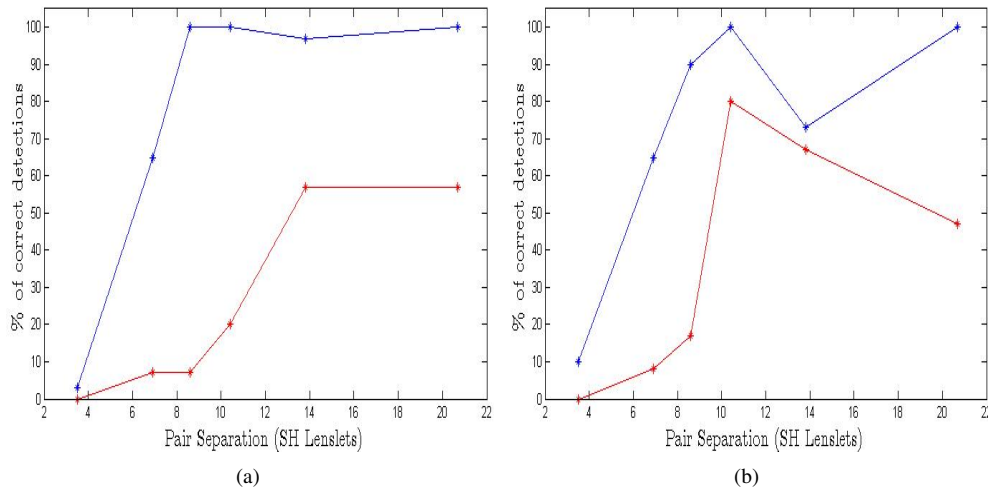| Fried's Parameter r_0 (cm)	80	32	21	11	8	5.7	4.7
Intensity Scintillation, σ_I^2	0.04	0.18	0.56	1.03	1.45	1.75	1.90
% Correct Detections	100	50	-	-	-	-	-
Sampling 1.68 cm/lenslet	17	7	-	-	-	-	-
% Correct Detections	90	60	27	13	-	-	-
Sampling 0.83 cm/lenslet	33	40	0	0	-	-	-
% Correct Detections	100	91	53	42	7	-	-
Sampling 0.55 cm/lenslet	62	56	18	0	0	-	-
% Correct Detections	100	98	87	79	53	60	60
Sampling 0.28 cm/lenslet	4	16	33	27	13	7	0

Fig. 8. The percentage of correct detection for the contour sum (red) and vortex potential methods (blue) against the spatial separation of vortices in terms of SH lenslets. The case of phase aberrations only, (a), and the case of the full optical field, (b), are shown for a coherence length $r_0 = 80$ cm and an intensity scintillation $\sigma_I^2 = 0.04$.

detection rate at lenlslet separation ≈ 14. This can be explained by the fact that one of the vortex pair was within 2 lenslets of the edge of the pupil. This has a negative effect on vortex detection because when a vortex is close to the edge of the pupil there are fewer slopes contributing to the vortex potential lessening the chances of detection.

However it can be deduced from the trend in Fig. 8 that the contour sum needs a greater spatial separation between vortices to enable optimum detection. While the vortex potential method needs ≈ 8 or 9 lenslets separation its optimum detection, $\geq 90\%$, the contour sum appears to need $\gtrsim 10$ lenslets to ensure it reaches its peak detection. The obvious explanation for this is that the one or more of the slope values used to calculate the contour sum are effected by the phase distortions induced by the nearby vortex which completes the pair. From Sec. 4.2

Table 4. The data used in Fig. 8(a) for the case of phase aberrations only. It shows the percentage of correct detections of vortex pairs for various SH lenslet separations.

Average Separation (SH Lenslets)	Vortex Potential % Correct Detection	Contour Sum % Correct Detection
3.5	3	0
6.9	65	7
8.6	100	7
10.4	100	20
13.8	97	57
20.7	100	57

$r_0 = 80$ cm and uniform intensity

it can be seen that these values corresponded to correct detection levels $\geq 90\%$, meaning that if the vortices are well enough separated they should be detected with a high degree of accuracy.

Table 5. The data used in Fig. 8(b) for the case of the full optical field. The percentage of correct detections of vortex pairs for various SH lenslet separations is presented.

Average Separation (SH Lenslets)	Vortex Potential % Correct Detection	Contour Sum % Correct Detection
3.5	10	0
6.9	65	8
8.6	90	17
10.4	100	80
13.8	73	67
20.7	100	47

$r_0 = 80$ cm and $\sigma_I^2 = 0.04$

5. Conclusions

Overall these results indicate that the vortex potential method is a strong and robust method for single vortex detection; often the percentage of correct detections in the field is greater than 90%, Figs 4 and 6. One obvious conclusion to draw from these results is that phase aberrations are the main factor in preventing vortex detection. This is because phase aberration is the main factor in causing an increase in SH spot width and motion which combine to make spot detection extremely difficult at certain SH sampling levels. Eventually these effects overcome the dynamic range of the SHWFS, meaning that no slope values can be calculated, and correspondingly the vortex detection rate drops to zero. This is seen for the wavefronts with phase aberrations only and those with phase aberrations and intensity scintillations. Any negative effect on vortex detection from the intensity scintillations does not begin until it enters the moderate regime, $\sigma_I^2 \gtrsim 0.5$, which can be seen by comparing the values in Table 3 to those in Table 2.

These results also show that the sampling of the SHWFS is key when attempting to detect optical vortices in a turbulent field, see Figs 5 and 7. By decreasing the amount of the field imaged by each lenslet the effective dynamic range of the SHWFS increases and allows Shack-Hartmann measurements to be made over a larger range of turbulence, overcoming one of the major factors limiting vortex detection. Increasing the sampling may not be a solution suitable

for all applications as it means, in the case of FSO communications, that light levels falling on the receiver would be further reduced. Also if the system has a fixed number of lenslets available it would decrease the field of view and if attempting to detect an optical vortex seeded, or naturally occurring, in the beam it would increase the chance of having the vortex wander outside of the pupil of the receiver.

It is obvious from these results that the contour sum method performs considerably worse under all conditions than the vortex potential method and performs especially poorly at high sampling levels. There are a number of reasons which explain the poor performance of the contour sum method but the major factor is that it uses only four slopes to calculate the detection metric. These four slopes are those closest to the centre of the vortex and as such are the most difficult to determine, with errors in position or non-detection more common. These errors increase as the SH sampling increases as the intensity null and phase singularity at the centre of the vortex are now spread out over a larger area on the lenslet array. There is also a larger percentage of false positives encountered in the contour sum method and they usually present themselves as being a negative and positive vortex in neighbouring lenslets, when only one vortex is actually present. While the overall optimum detection threshold for the contour sum method was ascertained, from reviewing the data shown here it is possible that the optimum threshold for detection changes with turbulence and may need to be adapted for each distinct turbulence level. It should also be noted that if looking to detect purely the overall vortex charge in a field the conotour sum method could be widened to a larger contour, instead of just four. This would overcome the main drawback of the method and make it more global but it woud lose spatial detection accuracy.

When detecting vortex pairs it can be seen that the vortex potential method outperforms the contour sum method. The vortex potential method needs only ≈ 8 or 9 lenslets separation for peak detection, $\geq 90\%$, whereas the contour sum needs $\gtrsim 10$ lenslets to reache its peak detection. The choice of Shack-Hartmann sampling is again crucial, by increasing the sampling the vortex pairs have a larger spatial separation in terms of SH lenslets. If the aim is to detect all of the vortices in a field this would be the route to take, however, if vortex pairs which are very close together are to be ignored then decreasing the sampling to a level where the pairs cannot be separated could be worthwhile. It should also be noted that the detection rate of vortices in a pair, with regard to the degree of turbulence and scintillation, mirrors that of single vortices once they are separated enough to be well detected.

Acknowledgments